Single-Loop Realization of Arbitrary Nonadiabatic Holonomic Single-Qubit Quantum Gates in a Superconducting Circuit

Y. Xu,[1] W. Cai,[1] Y. Ma,[1] X. Mu,[1] L. Hu,[1] Tao Chen,[2] H. Wang,[1] Y. P. Song,[1] Zheng-Yuan Xue,[2,*] Zhang-qi Yin,[1,†] and L. Sun[1,‡]

[1]*Center for Quantum Information, Institute for Interdisciplinary Information Sciences, Tsinghua University, Beijing 100084, China*

[2]*Guangdong Provincial Key Laboratory of Quantum Engineering and Quantum Materials, and School of Physics and Telecommunication Engineering, South China Normal University, Guangzhou 510006, China*

(Received 25 April 2018; published 11 September 2018)

Geometric phases are noise resilient, and thus provide a robust way towards high-fidelity quantum manipulation. Here we experimentally demonstrate arbitrary nonadiabatic holonomic single-qubit quantum gates for both a superconducting transmon qubit and a microwave cavity in a single-loop way. In both cases, an auxiliary state is utilized, and two resonant microwave drives are simultaneously applied with well-controlled but varying amplitudes and phases for the arbitrariness of the gate. The resulting gates on the transmon qubit achieve a fidelity of 0.996 characterized by randomized benchmarking and the ones on the cavity show an averaged fidelity of 0.978 based on a full quantum process tomography. In principle, a nontrivial two-qubit holonomic gate between the qubit and the cavity can also be realized based on our presented experimental scheme. Our experiment thus paves the way towards practical nonadiabatic holonomic quantum manipulation with both qubits and cavities in a superconducting circuit.

DOI: 10.1103/PhysRevLett.121.110501

High-fidelity quantum manipulation is essential for large scale quantum computation. However, as quantum systems are fragile under noises from either the surrounding environment or the control fields, error-resilient manipulations of quantum states are preferable. Geometric phases [1,2] depend only on the global properties of the evolution trajectories, and thus have built-in noise-resilient features against certain local noises [3–7]. Therefore, they can naturally be used to achieve high-fidelity quantum gates. Consequently, considerable interest has been paid to various applications of geometric phases in quantum computation [8].

Because of the noncommutativity, non-Abelian geometric phases are natural for the so-called holonomic quantum computation [9]. Schemes based on the adiabatic evolution of the non-Abelian geometric phases have been proposed on a variety of systems for quantum computation [10–15]. However, these schemes are rather difficult for experimental realization as they rely on complicated control over multilevel systems. Meanwhile, the gates are based on the rather slow adiabatic quantum dynamics and thus decoherence can induce considerable errors. Therefore, it is desirable to implement quantum gates with nonadiabatic evolutions [16]. Recently, much attention has been paid to the nonadiabatic holonomic quantum computation with three-level systems [17,18]. Compared to the adiabatic ones, this type of new scheme is fast and easy to realize, and has been experimentally demonstrated in superconducting circuits [19,20], nuclear magnetic resonance (NMR) [21], and nitrogen-vacancy centers in diamond [22–24].

More importantly, arbitrary single-qubit holonomic gates can be achieved in a single-loop evolution, i.e., a single closed loop evolution in parameter space [25–27]. This simplifies gate sequences in practical quantum information processing compared with the original proposal [17], where two sequential gates are required for an arbitrary single-qubit gate. In the last year, the single-loop scheme has been experimentally demonstrated in NMR [28] and nitrogen-vacancy centers in diamond with off-resonance drives [29], which are basically incompatible with pulse shaping and experimentally difficult. Therefore, single-loop schemes with resonant drives are generally required to use shaped pulses to reduce errors.

Here, with a circuit quantum electrodynamics architecture [30–34] we experimentally demonstrate arbitrary nonadiabatic holonomic single-qubit gates for both a superconducting transmon qubit and a microwave photonic qubit in a single-loop way. This is realized by varying the amplitudes and phases of a two-tone resonant microwave drive [27]. Besides transmon qubits, photonic qubits in a microwave cavity are also desirable for quantum information processing because of their long coherence times [35,36] and ease of realizing quantum error correction [37,38]. In our realization, the gates on the transmon qubit achieve a fidelity of 0.996 characterized by randomized benchmarking (RB), also consistent with the results from a full quantum process tomography (QPT); the gates on the

cavity show an averaged fidelity of 0.978 based on a full QPT. Besides local noises, the demonstrated holonomic gates on the qubit are also robust against control amplitude errors and qubit frequency shifts induced by crosstalk [39], which become prominent as qubit coherence properties are improved and the size of the quantum system increases. The holonomic gates on the cavity provide an alternative means of arbitrary control over Fock states, which also could be robust against experimental noises as the ones on the qubit.

We first address the implementation of arbitrary single-qubit holonomic gates on a superconducting transmon qubit in the $\{|g\rangle, |f\rangle\}$ subspace, as shown in Fig. 1(a). Here, $|g\rangle$, $|e\rangle$, and $|f\rangle$ denote the three lowest energy levels of the transmon qubit; $|e\rangle$ is an auxiliary state and remains unoccupied before and after the gate operation. Our scheme consists of two microwave fields resonantly coupled to the sequential transitions $|g\rangle \leftrightarrow |e\rangle$ and $|e\rangle \leftrightarrow |f\rangle$ of the transmon qubit, as described by

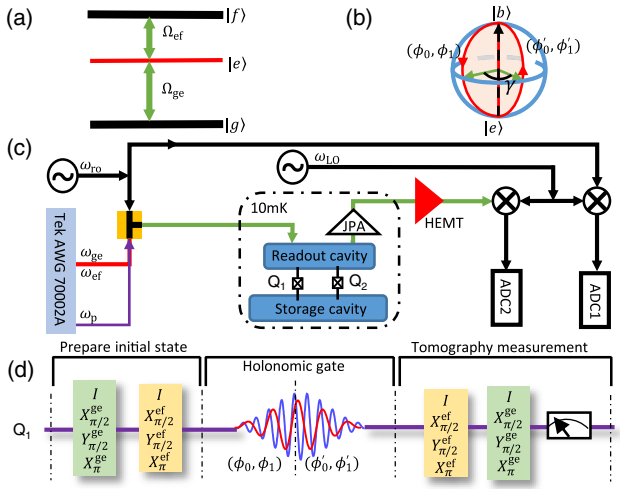

FIG. 1. Single-loop single-qubit holonomic gates. (a) Two microwave fields are resonantly coupled to the $|g\rangle \leftrightarrow |e\rangle$ and $|e\rangle \leftrightarrow |f\rangle$ transitions of a transmon qubit to generate arbitrary single-qubit holonomic gates in the $\{|g\rangle, |f\rangle\}$ subspace. The first excited state $|e\rangle$ is an auxiliary level. (b) Bloch sphere representation of the holonomic gate: a combination of two microwave fields, with two different sets of phases for the first and the second half of the gate operation, equivalently drives the bright state $|b\rangle$ to the auxiliary state $|e\rangle$ and then back with an additional phase, while the dark state $|d\rangle$ remains unchanged. (c) Simplified experimental setup. Two transmon qubits in two microwave trenches are coupled to two microwave cavities, one for readout and the other one for storage. The qubit holonomic gates are demonstrated with Q_1, while the cavity holonomic gates are realized with the Fock states $\{|0\rangle, |1\rangle\}$ in the storage cavity facilitated by both qubits (Fig. 4). (d) QPT is used to characterize the performance of the arbitrary holonomic gates. Arbitrary initial states are prepared with sequential pulses on $|g\rangle \leftrightarrow |e\rangle$ and $|e\rangle \leftrightarrow |f\rangle$ transitions. Nine sequential prerotation pulses on the qubit are performed before the final measurement to obtain the transmon's full state tomography with three levels.

$$\begin{aligned}\mathcal{H}_1 &= \Omega_{ge}(t)e^{i\phi_0}|g\rangle\langle e| + \Omega_{ef}(t)e^{i\phi_1}|f\rangle\langle e| + \text{H.c.} \\ &= \Omega(t)e^{i(\phi_1-\pi)}\left(\sin\frac{\theta}{2}e^{i\phi}|g\rangle - \cos\frac{\theta}{2}|f\rangle\right)\langle e| + \text{H.c.},\end{aligned} \tag{1}$$

where $\Omega_{ge}(t)$ and $\Omega_{ef}(t)$ are the time-dependent amplitudes of the two microwave drives with the corresponding initial phases ϕ_0 and ϕ_1; $\phi = \phi_0 - \phi_1 + \pi$, $\Omega(t) = \sqrt{\Omega_{ge}^2(t) + \Omega_{ef}^2(t)}$, and $\tan(\theta/2) = \Omega_{ge}(t)/\Omega_{ef}(t)$. As seen in Eq. (1), the quantum dynamics is captured by the resonant coupling between the bright state $|b\rangle = \sin(\theta/2)e^{i\phi}|g\rangle - \cos(\theta/2)|f\rangle$ and the auxiliary state $|e\rangle$, while the dark state $|d\rangle = \cos(\theta/2)|g\rangle + \sin(\theta/2)e^{-i\phi}|f\rangle$ is decoupled. Under the cyclic evolution condition, $\int_0^T \Omega(t)dt = \pi$, one can obtain a quantum gate depending on θ and/or ϕ. Meanwhile, since there is no transition between $|d\rangle$ and $|b\rangle$ states when θ is time independent and also no dynamical phases due to the on-resonance drives, the obtained gates are holonomic [17].

To achieve a universal set of single-qubit holonomic gates in a single-loop way [27], we divide the evolution time T into two equal halves and choose $\phi_0 = \phi$, $\phi_1 = \pi$ for $t \in [0, T/2]$ and $\phi_0{}' = \phi + \gamma - \pi$, $\phi_1{}' = \gamma$ for $t \in [T/2, T]$, such that the Hamiltonians during these two halves are $\mathcal{H}_A = \Omega(t)(|b\rangle\langle e| + |e\rangle\langle b|)$ and $\mathcal{H}_B = -\Omega(t)(e^{i\gamma}|b\rangle\langle e| + e^{-i\gamma}|e\rangle\langle b|)$, respectively. Geometrically, the two evolutions coincide at two poles in the Bloch sphere, and the cyclic geometric phase is illustrated as the red slice contour in Fig. 1(b). Therefore, in the qubit subspace $\{|g\rangle, |f\rangle\}$, the obtained holonomic single-qubit gate is

$$\begin{aligned}U_1(\theta,\gamma,\phi) &= \begin{pmatrix} \cos\frac{\gamma}{2} - i\sin\frac{\gamma}{2}\cos\theta & -i\sin\frac{\gamma}{2}\sin\theta e^{i\phi} \\ -i\sin\frac{\gamma}{2}\sin\theta e^{-i\phi} & \cos\frac{\gamma}{2} + i\sin\frac{\gamma}{2}\cos\theta \end{pmatrix} \\ &= \exp\left(-i\frac{\gamma}{2}\mathbf{n}\cdot\sigma\right),\end{aligned} \tag{2}$$

which describes a rotation operation around the axis $\mathbf{n} = (\sin\theta\cos\phi, \sin\theta\sin\phi, \cos\theta)$ by an angle γ, up to a global phase factor $\exp(i\gamma/2)$.

In our experiment, two superconducting transmon qubits are dispersively coupled to two three-dimensional cavities [50–53], as shown in Fig. 1(c). The $|g\rangle \leftrightarrow |e\rangle$ and $|e\rangle \leftrightarrow |f\rangle$ transition frequencies of the two qubits Q_1 and Q_2 are $\omega_{ge1}/2\pi = 5.036$ GHz and $\omega_{ef1}/2\pi = 4.782$ GHz, $\omega_{ge2}/2\pi = 5.605$ GHz, and $\omega_{ef2}/2\pi = 5.367$ GHz, respectively. One of the cavities with a transition frequency of $\omega_r/2\pi = 8.540$ GHz is connected to a Josephson parametric amplifier for a fast and high-fidelity joint readout of the two-qubit states [54–57]. The other cavity with a transition frequency of $\omega_s/2\pi = 7.614$ GHz is utilized for storage and manipulation of the photonic states and for implementing

the holonomic gates between Fock states $|0\rangle$ and $|1\rangle$ as is discussed below. In the following, we ignore the readout cavity and the cavity refers to the storage cavity. More details about the device parameters can be found in Ref. [39].

We now demonstrate the realization of the arbitrary holonomic gates in a single-loop way with transmon qubit Q_1 based on the procedure discussed above. The envelopes of the two drives are truncated Gaussian pulses with a total width of $4\sigma = 120$ ns. We characterize the holonomic single-qubit gates by a full QPT including all three levels, $|g\rangle$, $|e\rangle$, and $|f\rangle$ [39–41]. The experimental pulse sequence is shown in Fig. 1(d). To evaluate the QPT, we have used both attenuated and unattenuated χ matrix fidelities, which are respectively defined as $F_{\mathrm{att}} = |\mathrm{Tr}(\chi_{\mathrm{exp}}\chi_{\mathrm{th}}^{\dagger})|$ and $F_{\mathrm{unatt}} = |\mathrm{Tr}(\chi_{\mathrm{exp}}\chi_{\mathrm{th}}^{\dagger})|/\sqrt{\mathrm{Tr}(\chi_{\mathrm{exp}}\chi_{\mathrm{exp}}^{\dagger})\mathrm{Tr}(\chi_{\mathrm{th}}\chi_{\mathrm{th}}^{\dagger})}$ [21,58,59], where χ_{exp} is the experimental process matrix and χ_{th} is the corresponding ideal process matrix. The latter fidelity can ignore the errors due to signal loss, e.g., the errors in state preparations and measurements. Figure 2(a) shows F_{unatt} of the gates as a function of both θ and γ with $\phi = 0$, and the averaged fidelity $\bar{F}_{\mathrm{unatt}} = 0.994$. Energy relaxation and dephasing of both excited states and nonperfect microwave drives can cause a population leakage outside the computation subspace $\{|g\rangle, |f\rangle\}$ to the auxiliary $|e\rangle$ state. This leakage can be characterized by the trace of the reduced process matrix χ_r, which describes the process only involving $|g\rangle$ and $|f\rangle$ and ignores any operators acting on the auxiliary state $|e\rangle$ [39]. Figure 2(b) shows the traces of χ_r originated from the measured χ_{exp} whose fidelities are shown in Fig. 2(a). The high value (0.992) of the averaged trace indicates that there is nearly no leakage outside the computation subspace for the holonomic gates on the transmon qubit. χ_r of four example gates are shown in Fig. 2(c) with $F_{\mathrm{unatt}} = 0.997$, 0.996, 0.996, and 0.996 respectively (the corresponding $F_{\mathrm{att}} = 0.976$, 0.980, 0.963, and 0.988).

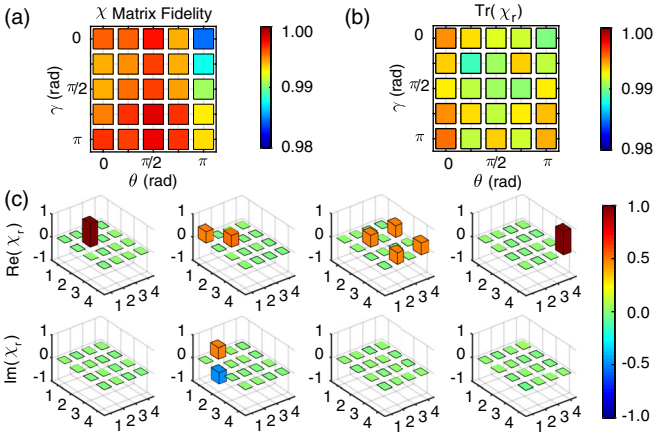

FIG. 2. QPT of the single-qubit holonomic gates. (a) Unattenuated χ matrix fidelity F_{unatt} of the single-qubit holonomic gates $U_1(\theta, \gamma, \phi)$ with different θ and γ while $\phi = 0$. The averaged fidelity $\bar{F}_{\mathrm{unatt}} = 0.994$ while the averaged attenuated fidelity $\bar{F}_{\mathrm{att}} = 0.975$. (b) The traces of the reduced process matrix χ_r as a function of both θ and γ with $\phi = 0$. The averaged trace is 0.992, indicating small leakage outside the computation subspace $\{|g\rangle, |f\rangle\}$. (c) Bar charts of the real and imaginary parts of χ_r of four specific gates: $X_\pi = U_1(\pi/2, \pi, 0)$, $X_{\pi/2} = U_1(\pi/2, \pi/2, 0)$, $H = U_1(\pi/4, \pi, 0)$, and $Z_\pi = U_1(0, \pi, 0)$, where R_φ denotes a rotation of the qubit by an angle φ along the axis R and H represents the Hadamard gate. The numbers in the x and y axes correspond to the operators in the basis set $\{I, X, -iY, Z\}$ of the $\{|g\rangle, |f\rangle\}$ subspace. The solid black outlines are for the ideal gates.

Another regular way to extract gate fidelity only without relying on perfect state preparations and measurements is RB [60–64]. An agreement between F_{unatt} and the fidelity from RB should provide more confidence on the gate performance. We utilize the Clifford-based RB and the experimental sequences are shown in Fig. 3(a), where we perform both a reference RB experiment and an interleaved RB experiment. The results of the four holonomic gates presented in Fig. 2(c) are shown in Fig. 3(b). Each Clifford gate is realized by choosing specific parameters θ, γ, and ϕ. The reference RB experiment gives an average gate fidelity of the single-qubit holonomic gates in the Clifford group $F_{\mathrm{avg}} = 0.996$. The measured gate fidelities of the four specific holonomic gates X_π, $X_{\pi/2}$, H, and Z_π are 0.998, 0.996, 0.997, and 0.995, respectively. These fidelities are consistent with the measured F_{unatt}, thus validating F_{unatt} as a good measure of gate performance. The loss of fidelity is mainly from the decoherence of both $|e\rangle$ and $|f\rangle$ of the

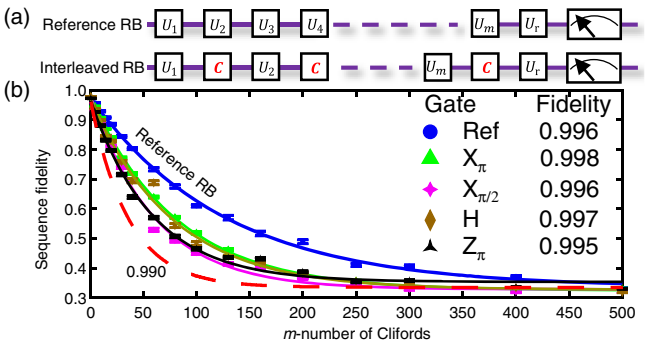

FIG. 3. RB of the single-qubit holonomic gates. (a) Sequences of both a reference RB experiment and an interleaved RB experiment. (b) The sequence fidelity decay as a function of the gate length m. The fidelity for each sequence length m is measured for $k = 100$ different random sequences with the standard deviation from the mean plotted as the error bars. Both curves are fitted with $F = Ap^m + B$ with different sequence decays $p = p_{\mathrm{ref}}$ and p_{gate}. The average gate fidelity per Clifford gate is $F_{\mathrm{avg}} = 1 - (1 - p_{\mathrm{ref}})/2 = 0.996$. The difference between the reference and the interleaved RB experiments gives the specific gate fidelity $F_{\mathrm{gate}} = 1 - (1 - p_{\mathrm{gate}}/p_{\mathrm{ref}})/2$. The red dashed line indicates the threshold for exceeding gate fidelity of 0.990.

transmon qubit, as confirmed by numerical simulations based on QuTiP in Python [65,66].

In addition to the implementation of holonomic gates on the transmon qubit, we also realize holonomic operations on the cavity Fock states following a similar scheme. As shown in Fig. 4(a), the holonomic gates are implemented by using a selective two-photon transition drive $\Omega_1 e^{i\omega_d t}$ on qubit Q_1 conditional on only zero photon in the cavity and a cavity-assisted Raman transition drive $\Omega_2 e^{i\omega_p t}$ between $|1g\rangle$ and $|0f\rangle$ [67,68]. Here the drive frequencies $\omega_d = (\omega_{ge1} + \omega_{ef1})/2$, $\omega_p = \omega_{ge1} + \omega_{ef1} - \omega_s$, and Ω_1 and Ω_2 are the corresponding drive strengths. In the joint state notation, the numbers represent the Fock states in the cavity and the letters correspond to the states of qubit Q_1.

Similarly, the above two drives together generate the following effective Hamiltonian [27,67]:

$$\begin{aligned}\mathcal{H}_2 &= \tilde{g}_1|0g\rangle\langle 0f| + \tilde{g}_2|1g\rangle\langle 0f| + \text{H.c.} \\ &= \tilde{g}\left(\sin\frac{\theta}{2}e^{i\phi}|0g\rangle - \cos\frac{\theta}{2}|1g\rangle\right)\langle 0f| + \text{H.c.}, \quad (3)\end{aligned}$$

where, $\tilde{g}_1$ and $\tilde{g}_2$ are the effective coupling strengthes of the two drives, and $\tilde{g} = \sqrt{\tilde{g}_1^2 + \tilde{g}_2^2}$, $\tilde{g}_1/\tilde{g}_2 = \tan(\theta/2)e^{i\phi}$. To validate the above Hamiltonian, $\tilde{g}_1$ of the two-photon transition drive should be much smaller than the dispersive shifts between qubit Q_1 and the cavity. In the experiment, both the two-photon transition drive and the Raman transition drive are set to have the same pulse envelope (a wide square pulse with sine squared ramp-up and ramp-down edges) to keep the two drives synchronized and the ratio of two amplitudes fixed. Both $\tilde{g}_1$ and $\tilde{g}_2$ are carefully calibrated with square pulses with different amplitudes [39]. We have also carefully taken into account the ac-Stark shifts under the strong external drives to eliminate the possible dynamical phases [39]. Similarly to the transmon qubit holonomic gates, by adjusting the ratios of $\tilde{g}_1$ and $\tilde{g}_2$, which lead to different θ and ϕ, we can realize arbitrary holonomic gates $U_1(\theta, \gamma, \phi)$ on the basis $\{|0g\rangle, |1g\rangle\}$, i.e., the Fock state basis $\{|0\rangle, |1\rangle\}$. As a demonstration, here we fix $\gamma = \pi$ and realize the holonomic gate $U_2(\theta, \phi) = \left(\begin{smallmatrix}\cos\theta & \sin\theta e^{i\phi} \\ \sin\theta e^{-i\phi} & -\cos\theta\end{smallmatrix}\right)$.

We characterize $U_2(\theta, \phi)$ with full QPT as well, and the results are shown in Fig. 4(b). To make the preparation and characterization of the cavity state easier, we instead use qubit Q_2 to facilitate an encoding and decoding process of the cavity state. The encoding and decoding processes are realized with a similar Raman transition drive between qubit Q_2 and the cavity as illustrated in Fig. 4(a). We choose four different gates X_π, Y_π, H_1, and H_2, and perform QPT of these gates. The experimental process matrices χ_{exp} are shown in Fig. 4(c). The averaged experimental attenuated and unattenuated process fidelities of these holonomic gates are $\bar{F}_{\text{att}} = 0.879$ and $\bar{F}_{\text{unatt}} = 0.978$, respectively. The infidelities of the

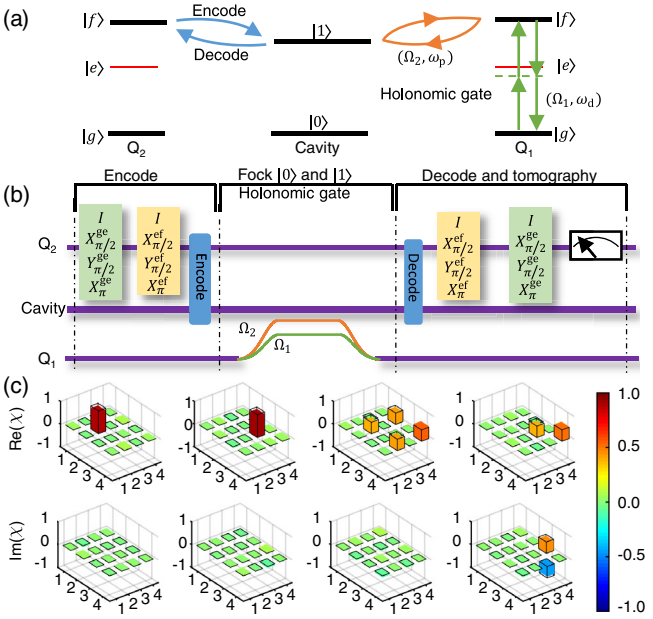

FIG. 4. Holonomic gates for cavity Fock state subspace $\{|0\rangle, |1\rangle\}$. (a) Illustration of the holonomic gates for Fock states, as well as the encoding and decoding processes. The holonomic gates are implemented by using a selective two-photon transition drive $\Omega_1 e^{i\omega_d t}$ on qubit Q_1 and a cavity-assisted Raman transition drive $\Omega_2 e^{i\omega_p t}$ between $|1g\rangle$ and $|0f\rangle$. The encoding and decoding processes are realized with a swap operation between qubit Q_2 and the cavity mode through a Raman transition drive similar to that for the gate. (b) Experimental sequence to perform QPT of the holonomic gates in the Fock $\{|0\rangle, |1\rangle\}$ subspace. (c) Bar charts of the real and imaginary parts of the process χ matrices for the whole process, including both the encoding and decoding processes, with the following gates: $X_\pi = U_2(\pi/2, 0)$, $Y_\pi = U_2(\pi/2, \pi/2)$, $H_1 = U_2(\pi/4, 0)$, and $H_2 = U_2(\pi/4, \pi/2)$. The attenuated and unattenuated process fidelities for these gates are 0.880, 0.881, 0.877, 0.879 and 0.990, 0.990, 0.970, 0.962, respectively. The numbers in the x and y axes correspond to the operators in the basis set $\{I, X, -iY, Z\}$. The solid black outlines are for the ideal gates.

holonomic gates for Fock states are mainly limited by the encoding and decoding errors (including the initial state preparation and final measurement errors), decoherence process during the gate, and imperfections of the control pulses. As a reference, the process fidelity of the encoding and decoding processes only without any gate is 0.95 (an error of 5%). The dissipation and dephasing of the two excited states $|e\rangle$ and $|f\rangle$ during the gate process can induce an additional infidelity of 5%–6% due to the long gate duration time. These two dominant error budgets are consistent with the measured attenuated fidelities. A higher fidelity gate can be achieved with a shorter gate operation time under a larger dispersive shift.

To achieve a universal quantum computation, two-qubit gates are necessary. A nontrivial two-qubit holonomic gate between the qubit and the cavity can, in principle, be

realized in a similar way to the single-qubit gates, i.e., by using two resonant selective pulses on $|g\rangle \leftrightarrow |e\rangle$ and $|e\rangle \leftrightarrow |f\rangle$ transitions, respectively, conditional on only zero photon in the cavity. Then the effective Hamiltonian is $\mathcal{H}_3 = \Omega_{ge}(t)e^{i\phi_0}|0g\rangle\langle 0e| + \Omega_{ef}e^{i\phi_1}(t)|0f\rangle\langle 0e| + \text{H.c.}$. A nontrivial two-qubit holonomic gate in the subspace $\{|0g\rangle, |0f\rangle, |1g\rangle, |1f\rangle\}$ can then be realized with the form of $U_3(\theta,\gamma,\phi) = \left(\begin{smallmatrix} U_1(\theta,\gamma,\phi) & 0 \\ 0 & I \end{smallmatrix}\right)$.

In conclusion, in a circuit quantum electrodynamics architecture we have experimentally demonstrated high-fidelity arbitrary nonadiabatic holonomic single-qubit gates for both a superconducting transmon qubit and a microwave cavity in a single-loop way. Moreover, our method can be generalized to achieve holonomic gates between the nearest Fock states $|n\rangle$ and $|n+1\rangle$, if the resonant drives are on $|n,g\rangle \leftrightarrow |n,f\rangle$ and $|n+1,g\rangle \leftrightarrow |n,f\rangle$ transitions. Combining these gates, we can realize full holonomic control of both the transmon qubit and the cavity mode [42,69–72], which has important applications in cavity-assisted quantum information processing and high-precision measurements [73]. Our experiment thus opens the door to implement holonomic manipulations of both qubits and cavities in a superconducting circuit. In addition, the $\{|g\rangle, |f\rangle\}$ encoding is critical for the recently realized distributed quantum information processing [68,74] and fault-tolerant measurement of a quantum error syndrome [75]; our holonomic gates therefore can be important and readily used in these two directions.

This work was supported by the National Key R&D Program of China (Grants No. 2017YFA0304303 and No. 2016YFA0301803) and National Natural Science Foundation of China (Grants No. 11474177, No. 11874156, and No. 61771278). L. S. also acknowledges the support of the Thousand Youth Fellowship program in China. L. S. also thanks R. Vijay and his group for help on the parametric amplifier measurements.

Note added.—Recently, we became aware of a similar implementation in a different system [76], but with a lower average gate fidelity due to the short coherence times of the auxiliary excited state.

*zyxue83@163.com
†yinzhangqi@tsinghua.edu.cn
‡luyansun@tsinghua.edu.cn

[1] M. V. Berry, Proc. R. Soc. A **392**, 45 (1984).
[2] F. Wilczek and A. Zee, Phys. Rev. Lett. **52**, 2111 (1984).
[3] S.-L. Zhu and P. Zanardi, Phys. Rev. A **72**, 020301 (2005).
[4] P. Solinas, M. Sassetti, P. Truini, and N. Zanghì, New J. Phys. **14**, 093006 (2012).
[5] M. Johansson, E. Sjöqvist, L. M. Andersson, M. Ericsson, B. Hessmo, K. Singh, and D. M. Tong, Phys. Rev. A **86**, 062322 (2012).
[6] S. Berger, M. Pechal, A. A. Abdumalikov, C. Eichler, L. Steffen, A. Fedorov, A. Wallraff, and S. Filipp, Phys. Rev. A **87**, 060303 (2013).
[7] C. G. Yale, F. J. Heremans, B. B. Zhou, A. Auer, G. Burkard, and D. D. Awschalom, Nat. Photonics **10**, 184 (2016).
[8] E. Sjöqvist, Physics **1**, 35 (2008).
[9] P. Zanardi and M. Rasetti, Phys. Lett. A **264**, 94 (1999).
[10] L. Duan, J. I. Cirac, and P. Zoller, Science **292**, 1695 (2001).
[11] J. Pachos, P. Zanardi, and M. Rasetti, Phys. Rev. A **61**, 010305 (1999).
[12] L.-A. Wu, P. Zanardi, and D. A. Lidar, Phys. Rev. Lett. **95**, 130501 (2005).
[13] Z. Q. Yin, F. L. Li, and P. Peng, Phys. Rev. A **76**, 062311 (2007).
[14] I. Kamleitner, P. Solinas, C. Müller, A. Shnirman, and M. Möttönen, Phys. Rev. B **83**, 214518 (2011).
[15] V. V. Albert, C. Shu, S. Krastanov, C. Shen, R.-B. Liu, Z.-B. Yang, R. J. Schoelkopf, M. Mirrahimi, M. H. Devoret, and L. Jiang, Phys. Rev. Lett. **116**, 140502 (2016).
[16] Y. Aharonov and J. Anandan, Phys. Rev. Lett. **58**, 1593 (1987).
[17] E. Sjöqvist, D. M. Tong, M. Andersson, B. Hessmo, M. Johansson, and K. Singh, New J. Phys. **14**, 103035 (2012).
[18] G. F. Xu, J. Zhang, D. M. Tong, E. Sjöqvist, and L. C. Kwek, Phys. Rev. Lett. **109**, 170501 (2012).
[19] A. A. Abdumalikov, J. M. Fink, K. Juliusson, M. Pechal, S. Berger, A. Wallraff, and S. Filipp, Nature (London) **496**, 482 (2013).
[20] D. J. Egger, M. Ganzhorn, G. Salis, A. Fuhrer, P. Mueller, P. K. Barkoutsos, N. Moll, I. Tavernelli, and S. Filipp, arXiv:1804.04900.
[21] G. Feng, G. Xu, and G. Long, Phys. Rev. Lett. **110**, 190501 (2013).
[22] C. Zu, W. Wang, L. He, W. Zhang, C. Y. Dai, F. Wang, and L. M. Duan, Nature (London) **514**, 72 (2014).
[23] S. Arroyocamejo, A. Lazariev, S. W. Hell, and G. Balasubramanian, Nat. Commun. **5**, 4870 (2014).
[24] Y. Sekiguchi, N. Niikura, R. Kuroiwa, H. Kano, and H. Kosaka, Nat. Photonics **11**, 309 (2017).
[25] G. F. Xu, C. L. Liu, P. Z. Zhao, and D. M. Tong, Phys. Rev. A **92**, 052302 (2015).
[26] E. Herterich and E. Sjöqvist, Phys. Rev. A **94**, 052310 (2016).
[27] Z.-P. Hong, B.-J. Liu, J.-Q. Cai, X.-D. Zhang, Y. Hu, Z. D. Wang, and Z.-Y. Xue, Phys. Rev. A **97**, 022332 (2018).
[28] H. Li, Y. Liu, and G. Long, Sci. China: Phys., Mech. Astron. **60**, 080311 (2017).
[29] B. B. Zhou, P. C. Jerger, V. O. Shkolnikov, F. J. Heremans, G. Burkard, and D. D. Awschalom, Phys. Rev. Lett. **119**, 140503 (2017).
[30] A. Wallraff, D. I. Schuster, A. Blais, L. Frunzio, R.-S. Huang, J. Majer, S. Kumar, S. M. Girvin, and R. J. Schoelkopf, Nature (London) **431**, 162 (2004).
[31] J. Clarke and F. K. Wilhelm, Nature (London) **453**, 1031 (2008).
[32] J. Q. You and F. Nori, Nature (London) **474**, 589 (2011).
[33] M. H. Devoret and R. J. Schoelkopf, Science **339**, 1169 (2013).

[34] X. Gu, A. F. Kockum, A. Miranowicz, Y. X. Liu, and F. Nori, Phys. Rep. **718–719**, 1 (2017).

[35] M. Reagor, H. Paik, G. Catelani, L. Sun, C. Axline, E. Holland, I. M. Pop, N. A. Masluk, T. Brecht, L. Frunzio *et al.*, Appl. Phys. Lett. **102**, 192604 (2013).

[36] M. Reagor, W. Pfaff, C. Axline, R. W. Heeres, N. Ofek, K. Sliwa, E. Holland, C. Wang, J. Blumoff, K. Chou *et al.*, Phys. Rev. B **94**, 014506 (2016).

[37] Z. Leghtas, G. Kirchmair, B. Vlastakis, R. J. Schoelkopf, M. H. Devoret, and M. Mirrahimi, Phys. Rev. Lett. **111**, 120501 (2013).

[38] M. H. Michael, M. Silveri, R. T. Brierley, V. V. Albert, J. Salmilehto, L. Jiang, and S. M. Girvin, Phys. Rev. X **6**, 031006 (2016).

[39] See Supplemental Material http://link.aps.org/supplemental/10.1103/PhysRevLett.121.110501 for a discussion of the experimental device and setup, system Hamiltonian, quantum process tomography, calibration of the two-photon transition and cavity-assisted transition drives, and noise-resilient feature of the holonomic gates, which includes Refs. [3–7,19,35,36,40–49].

[40] R. T. Thew, K. Nemoto, A. G. White, and W. J. Munro, Phys. Rev. A **66**, 012303 (2002).

[41] R. Bianchetti, S. Filipp, M. Baur, J. M. Fink, C. Lang, L. Steffen, M. Boissonneault, A. Blais, and A. Wallraff, Phys. Rev. Lett. **105**, 223601 (2010).

[42] R. W. Heeres, B. Vlastakis, E. Holland, S. Krastanov, V. V. Albert, L. Frunzio, L. Jiang, and R. J. Schoelkopf, Phys. Rev. Lett. **115**, 137002 (2015).

[43] J. Raftery, A. Vrajitoarea, G. Zhang, Z. Leng, S. J. Srinivasan, and A. A. Houck, arXiv:1703.00942.

[44] F. Motzoi, J. M. Gambetta, P. Rebentrost, and F. K. Wilhelm, Phys. Rev. Lett. **103**, 110501 (2009).

[45] J. M. Gambetta, F. Motzoi, S. T. Merkel, and F. K. Wilhelm, Phys. Rev. A **83**, 012308 (2011).

[46] M. J. Peterer, S. J. Bader, X. Jin, F. Yan, A. Kamal, T. J. Gudmundsen, P. J. Leek, T. P. Orlando, W. D. Oliver, and S. Gustavsson, Phys. Rev. Lett. **114**, 010501 (2015).

[47] M. D. Reed, Ph.D. thesis, Yale University, 2013.

[48] D. F. V. James, P. G. Kwiat, W. J. Munro, and A. G. White, Phys. Rev. A **64**, 052312 (2001).

[49] M. A. Nielsen and I. L. Chuang, *Quantum Computation and Quantum Information* (Cambridge University Press, Cambridge, 2000).

[50] H. Paik, D. I. Schuster, L. S. Bishop, G. Kirchmair, G. Catelani, A. P. Sears, B. R. Johnson, M. J. Reagor, L. Frunzio, L. I. Glazman *et al.*, Phys. Rev. Lett. **107**, 240501 (2011).

[51] B. Vlastakis, G. Kirchmair, Z. Leghtas, S. E. Nigg, L. Frunzio, S. M. Girvin, M. Mirrahimi, M. H. Devoret, and R. J. Schoelkopf, Science **342**, 607 (2013).

[52] L. Sun, A. Petrenko, Z. Leghtas, B. Vlastakis, G. Kirchmair, K. M. Sliwa, A. Narla, M. Hatridge, S. Shankar, J. Blumoff *et al.*, Nature (London) **511**, 444 (2014).

[53] K. Liu, Y. Xu, W. Wang, S.-B. Zheng, T. Roy, S. Kundu, M. Chand, A. Ranadive, R. Vijay, Y. Song *et al.*, Sci. Adv. **3**, e1603159 (2017).

[54] M. Hatridge, R. Vijay, D. H. Slichter, J. Clarke, and I. Siddiqi, Phys. Rev. B **83**, 134501 (2011).

[55] T. Roy, S. Kundu, M. Chand, A. M. Vadiraj, A. Ranadive, N. Nehra, M. P. Patankar, J. Aumentado, A. A. Clerk, and R. Vijay, Appl. Phys. Lett. **107**, 262601 (2015).

[56] A. Kamal, A. Marblestone, and M. H. Devoret, Phys. Rev. B **79**, 184301 (2009).

[57] K. W. Murch, S. J. Weber, C. Macklin, and I. Siddiqi, Nature (London) **502**, 211 (2013).

[58] Y. S. Weinstein, T. F. Havel, J. Emerson, and N. Boulant, J. Chem. Phys. **121**, 6117 (2004).

[59] J. Zhang, R. Laflamme, and D. Suter, Phys. Rev. Lett. **109**, 100503 (2012).

[60] E. Knill, D. Leibfried, R. Reichle, J. Britton, R. B. Blakestad, J. D. Jost, C. Langer, R. Ozeri, S. Seidelin, and D. J. Wineland, Phys. Rev. A **77**, 012307 (2008).

[61] J. M. Chow, J. M. Gambetta, L. Tornberg, J. Koch, L. S. Bishop, A. A. Houck, B. R. Johnson, L. Frunzio, S. M. Girvin, and R. J. Schoelkopf, Phys. Rev. Lett. **102**, 090502 (2009).

[62] E. Magesan, J. M. Gambetta, B. R. Johnson, C. A. Ryan, J. M. Chow, S. T. Merkel, M. P. da Silva, G. A. Keefe, M. B. Rothwell, T. A. Ohki *et al.*, Phys. Rev. Lett. **109**, 080505 (2012).

[63] E. Magesan, J. M. Gambetta, and J. Emerson, Phys. Rev. Lett. **106**, 180504 (2011).

[64] R. Barends, J. Kelly, A. Megrant, A. Veitia, D. Sank, E. Jeffrey, T. C. White, J. Mutus, A. G. Fowler, B. Campbell *et al.*, Nature (London) **508**, 500 (2014).

[65] J. R. Johansson, P. D. Nation, and F. Nori, Comput. Phys. Commun. **183**, 1760 (2012).

[66] J. R. Johansson, P. D. Nation, and F. Nori, Comput. Phys. Commun. **184**, 1234 (2013).

[67] S. Zeytinoğlu, M. Pechal, S. Berger, A. A. Abdumalikov, A. Wallraff, and S. Filipp, Phys. Rev. A **91**, 043846 (2015).

[68] M. Pechal, L. Huthmacher, C. Eichler, and S. Zeytinoğlu, A. A. Abdumalikov, S. Berger, A. Wallraff, and S. Filipp, Phys. Rev. X **4**, 041010 (2014).

[69] K. Vogel, V. M. Akulin, and W. P. Schleich, Phys. Rev. Lett. **71**, 1816 (1993).

[70] C. K. Law and J. H. Eberly, Phys. Rev. Lett. **76**, 1055 (1996).

[71] M. Hofheinz, H. Wang, M. Ansmann, R. C. Bialczak, E. Lucero, M. Neeley, A. D. O'Connell, D. Sank, J. Wenner, J. M. Martinis *et al.*, Nature (London) **459**, 546 (2009).

[72] W. Wang, L. Hu, Y. Xu, K. Liu, Y. Ma, S.-B. Zheng, R. Vijay, Y. P. Song, L.-M. Duan, and L. Sun, Phys. Rev. Lett. **118**, 223604 (2017).

[73] C. M. Caves, K. S. Thorne, R. W. P. Drever, V. D. Sandberg, and M. Zimmermann, Rev. Mod. Phys. **52**, 341 (1980).

[74] P. Kurpiers, P. Magnard, T. Walter, B. Royer, M. Pechal, J. Heinsoo, Y. Salathé, A. Akin, S. Storz, J.-C. Besse *et al.*, Nature (London) **558**, 264 (2018).

[75] S. Rosenblum, P. Reinhold, M. Mirrahimi, L. Jiang, L. Frunzio, and R. J. Schoelkopf, Science **361**, 266 (2018).

[76] N. Ishida, T. Nakamura, T. Tanaka, S. Mishima, H. Kano, R. Kuroiwa, Y. Sekiguchi, and H. Kosaka, Opt. Lett. **43**, 2380 (2018).